

EM-Based Estimation and Compensation of Phase Noise in Massive-MIMO Uplink Communications

Alberto Tarable and Francisco J. Escribano, *Senior Member, IEEE*

Abstract

Phase noise (PN) is a major disturbance in MIMO systems, where the contribution of different oscillators at the transmitter and the receiver side may degrade the overall performance and offset the gains offered by MIMO techniques. This is even more crucial in the case of massive MIMO, since the number of PN sources may increase considerably. In this work, we propose an iterative receiver based on the application of the expectation-maximization algorithm. We consider a massive MIMO framework with a general association of oscillators to antennas, and include other channel disturbances like imperfect channel state information and Rician block fading. At each receiver iteration, given the information on the transmitted symbols, steepest descent is used to estimate the PN samples, with an optimized adaptive step size and a threshold-based stopping rule. The results obtained for several test cases show how the bit error rate and mean square error can benefit from the proposed phase-detection algorithm, even to the point of reaching the same performance as in the case where no PN is present. Further analysis of the results allow to draw some useful trade-offs respecting final performance and consumption of resources.

Index Terms

Massive MIMO, EM Algorithm, Phase Noise, Iterative Decoding

I. INTRODUCTION

Massive MIMO [1] is a key enabling technique to achieve the large throughput required by current 5G cellular networks. In the massive MIMO concept, the base station (BS) is equipped with many more antennas than the number strictly needed to communicate with the users in its cell. Thanks to

Alberto Tarable is with the Consiglio Nazionale delle Ricerche, Istituto di Elettronica e di Ingegneria Informatica e delle Telecomunicazioni (CNR-IEIIT), Italy (e-mail: alberto.tarable@ieiit.cnr.it).

Francisco J. Escribano is with the Department of Signal Theory and Communications, Universidad de Alcalá, 28805 Alcalá de Henares, Spain (e-mail: francisco.escribano@uah.es).

this overabundance of antennas, users communicating in the same time-frequency resources can be distinguished by means of simple linear filter techniques, such as minimum mean-square error (MMSE) in the uplink, or maximum ratio transmission (MRT) [2] in the downlink. Such filters require channel state information (CSI) for all links, in order to behave properly. CSI is typically obtained through the transmission of pilots, which are inserted within the frame at regular time intervals, depending on the channel coherence time. Thus, in order to achieve the performance promised by massive MIMO, obtaining a good CSI estimation becomes of crucial importance.

In real systems, the channel seen at the receiver is time-varying not only because of mobility, either of the user equipments (UEs) or of the surrounding environment (e.g., scatterers, reflectors, etc.), but also because of hardware nonidealities. One of the most important impairments of this type is phase noise (PN) [3]. PN arises from instability in the oscillators and typically assumes the form of a multiplicative noise, whose effect in massive MIMO systems can become particularly severe, substantially harming the performance of the receiver filters. While, in principle, pilot transmission allows the estimation of actual PN, usually PN processes have a much faster time evolution than other forms of channel variations. Thus, between two pilot transmissions, the estimated PN becomes rapidly obsolete, i.e. information aging takes place.

In this paper, we deal with the problem of reducing the impact of PN in a single-cell massive MIMO uplink. In particular, we introduce a receiver that is able to approximate joint PN detection and demodulation by iterating between a phase detector and a demodulator/decoder. The entire receiver is based on the expectation-maximization (EM) algorithm. The receiver was originally introduced in [4] for a non-massive MIMO line-of-sight (LoS) system, where the proposed structure was shown to achieve excellent performance.

A. *Related work*

Several papers from the literature have faced the problem of PN in massive MIMO systems. A major distinction can be made between papers that deal with single-carrier transmission schemes and papers that deal with OFDM.

For massive MIMO-OFDM systems, the problem of PN is even more relevant than in single-carrier systems, as PN causes the loss of orthogonality of the subcarriers, giving rise to inter-carrier interference (ICI). Apart from the large bulk of literature regarding the impact of PN on non-massive MIMO-OFDM systems, the work in [5] specifically considers the uplink of a massive MIMO-OFDM system affected by

PN. Two extreme cases are considered, the synchronous case where a single oscillator is feeding all the M BS antennas, and the asynchronous case where each BS antenna is fed by a different oscillator. The ergodic capacity in the asymptotic limit $M \rightarrow \infty$ is computed and a Kalman filter is proposed to track the PN. Under a similar scenario, in [6] the authors derive lower bounds to the ergodic capacity for a finite value of M . In reference [7], a more composite PN model is introduced, in which the phase-locked loop (PLL) structure is taken into account to derive the PN statistics. It is shown that, while independent PN at each BS antenna is averaged out, a common PN component can give a substantial performance loss. In [8], the downlink of a massive MIMO-OFDM system is considered and the impact of PN on the performance of the zero-forcing and MRT precoders is characterized. The effect of imperfect CSI is also investigated. In [9], an iterative algorithm, based on variational EM, is proposed for compensation of PN in the uplink of massive MIMO-OFDM systems. Such algorithm performs joint channel and PN estimation.

For single-carrier systems, the authors in [10] consider the uplink of frequency-selective massive MIMO systems, with single-antenna users transmitting to the BS. Again, synchronous and asynchronous cases are considered for the PN at the BS. A time-reversal maximal-ratio combining is proposed, and its performance is analyzed. Asymptotically in M , the array gain is shown to be $O(\sqrt{M})$, as in the case without PN. In the non-asymptotic case, a dramatic worsening of performance due to PN is shown, with a further loss in the asynchronous case. The performance loss is also caused by the very simple receiver considered. The downlink of a frequency-flat massive MIMO system is studied in [11]. In the downlink, it is unlikely to introduce a PN estimation/tracking algorithm, due to the limited computational complexity of the UEs. In [11], the PN model at the BS is more general, supposing that an oscillator can feed several BS antennas. The effect of PN on the per-user SINR is evaluated, depending on the different linear precoder, i.e., zero-forcing (ZF), regularized ZF, or matched filter. It is shown that the performance loss increases with an increasing number of oscillators. In [12] a precoding scheme based on ZF with PN suppression is proposed for the downlink of a massive MIMO with time division duplexing (TDD). Because of reciprocity, the estimated uplink channel (obtained with a simple PN estimation scheme) is used in the downlink to form the ZF precoder. The work in [13] introduces an algorithm based on approximate Bayesian interference for symbol error reduction of the PN-impaired uplink of massive MIMO systems. Since the performance parameter of [13] is symbol error rate, it is not suitable for coded systems, as is considered in the present paper.

More recently, reference [14] investigates PN-affected massive MIMO systems in the mmWave band. The PN model is similar to the one considered in [7], with a common reference low-frequency oscillator that feeds all BS antennas, and a bank of PLLs, each feeding a subset of BS antennas, in order to raise the carrier frequency to mmWave band. Thus, there are two contributions to PN, one from the reference oscillator, common to all antennas, the other from the PLL voltage-controlled oscillator (VCO), which is independent for different antenna subsets. The first PN contribution is proven to be low-frequency and thus easily estimated, while the second term has a faster dynamics and thus turns out to be more problematic. The performance is characterized for MMSE filtering, when QPSK symbols are transmitted, yielding assessment of the PN impact on the output BER. In [15], the focus is on hybrid analog-digital schemes for mmWave massive MIMO, for which the sensitivity to PN and channel estimation errors is quantitatively analyzed. Hybrid analog-digital schemes are a way to reduce the number of RF chains, which is especially important at the mmWave band. Moreover, a comparison between the hybrid and the fully-digital scheme in terms of robustness with respect to PN is performed. In [16] the impact of PN on beamforming performance for mmWave massive MIMO systems is investigated.

On the other hand, a very recent flavor that is capturing the attention of the research community is related to cell-free massive MIMO systems. The work in [17] analyzes the impact of PN on the performance of cell-free massive MIMO systems, both for their uplink and their downlink, showing that end users suffer more than access points (APs) from PN. PN-aware power control is also studied. In [18], the spectral efficiency of a frequency-selective cell-free massive MIMO system with PN and imperfect channel estimation is studied, specifically when two linear low-complexity decoders, namely, time-reversal maximum-ratio combining and time-reversal large-scale fading decoding, are employed. Finally, it is worth noting that massive MIMO systems affected by PN have been studied in several particular applications, such as compressive channel estimation [19], PHY-layer authentication [20], or joint channel estimation and localization [21], among others.

In this paper, we consider the uplink of a single-carrier frequency-flat massive MIMO system. Thus, apart from the band, we are in a setup close to that of [14]. We consider independent PN processes for given antennas subsets, i.e., we neglect a common reference oscillator, whose PN contribution is proven in [14] to be easily estimated. The novelty of this work relies in a study of the performance improvement determined by an iterative receiver, which represents a viable, suboptimal implementation of a joint phase detector and demodulator/decoder. It is to be noted that some preliminary simulation results obtained with

the receiver proposed in this paper were shown in [22] to assess the effect of CSI aging.

Summarizing, the main contributions of this paper are as follows:

- We describe in detail the proposed receiver under a general setting where each oscillator at the transmitter and at the receiver can feed an arbitrary number of antennas, extending the receiver of [4];
- We derive the Bayesian Cramér-Rao Bound (BCRB) for this general setting, yielding a benchmark for the performance in terms of the mean-square error (MSE) of the proposed receiver;
- Through numerical simulations, we analyze the receiver performance both in terms of MSE and in terms of bit error rate (BER) in several realistic scenarios, including imperfect CSI;
- We conclude with several design rules both for the receiver and for the system, in order to achieve a given target performance.

The remaining of this paper is structured as follows. In Section II, we describe the system under consideration, with Subsection II-B devoted to the description of the pilot transmission scheme and of the assumptions made on channel estimation. In Section III, the EM-based receiver is described, with particular emphasis on the phase estimator (Subsection III-A) and a brief description of the MIMO demodulator (Subsection III-B). Section IV derives the Bayesian Cramér-Rao bound. Section V shows the simulation results, both in terms of MSE (Subsection V-A), BER (Subsection V-B), and average number of receiver iterations and steepest-descent steps (Subsection V-C), as well as looks into the algorithm complexity and latency (Subsection V-D). Finally, Section VI draws some conclusions.

II. SYSTEM DESCRIPTION

A. Overall channel model

The model we describe below, while general in nature, is specially suitable for the uplink of a wireless network in which several users (typically, with one or few transmit antennas each) transmit to a base station equipped with many antennas and able to sustain a relevant computational burden. This situation will (implicitly or explicitly, where corresponding) constitute our specific context throughout the article.

Consider an $N_t \times N_r$ massive MIMO channel with O_t oscillators at the transmitter (corresponding to a total of K users) and O_r oscillators at the receiver. Each transmit-side oscillator feeds $N_{o,t} = N_t/O_t$ antennas, while similarly $N_{o,r} = N_r/O_r$ receive antennas are fed by the same oscillator¹, as shown

¹Notice that an even more general scenario in which different oscillators may feed different numbers of antennas is compatible with our proposal. However, we chose not to pursue this case to avoid unnecessary notation mess.

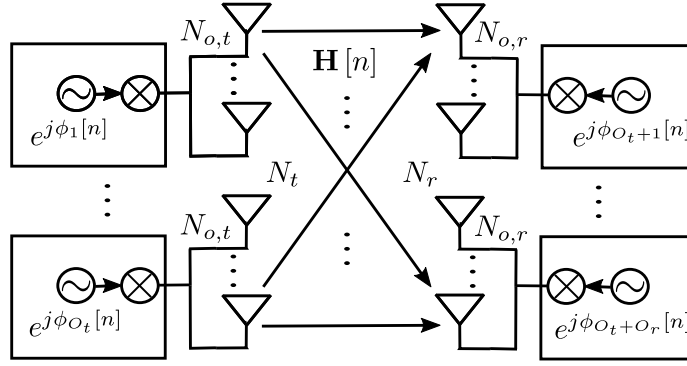


Fig. 1. Overall scheme of the MIMO channel and oscillator/antenna setup for the massive MIMO system.

in Fig. 1, where the general model for the MIMO channel and oscillator setup is detailed. Different oscillators introduce independent PN processes. The input-output relationship for the MIMO setup at time $n = 1, 2, \dots$ is given by

$$\mathbf{y}[n] = \mathbf{\Phi}_R[n] \mathbf{H}[n] \mathbf{\Phi}_T[n] \mathbf{x}[n] + \mathbf{z}[n], \quad (1)$$

where:

- $\mathbf{H}[n]$ is the $N_r \times N_t$ channel matrix at time n , whose statistical characterization will be described in more detail below and in Subsection V-A;
- $\mathbf{\Phi}_T[n] = \text{diag}(e^{j\phi_1[n]}, \dots, e^{j\phi_{O_t}[n]}) \otimes \mathbf{I}_{N_{o,t}}$ and $\mathbf{\Phi}_R[n] = \text{diag}(e^{j\phi_{O_t+1}[n]}, \dots, e^{j\phi_{O_t+O_r}[n]}) \otimes \mathbf{I}_{N_{o,r}}$ are the diagonal matrices of transmit and receive phase-noise coefficients at time n , respectively, assumed to be unknown at both sides; notice that we have assumed that oscillator i , $i = 1, \dots, O_t$ feeds transmit antennas $(i-1)N_{o,t} + j$, $j = 1, \dots, N_{o,t}$, while oscillator $O_t + i$, $i = 1, \dots, O_r$ feeds receive antennas $(i-1)N_{o,r} + j$, $j = 1, \dots, N_{o,r}$;
- $\mathbf{x}[n]$ is the column vector of the N_t transmitted modulated symbols at time n , each of them having average energy E_s ;
- $\mathbf{y}[n]$ is the column vectors of the N_r received samples at time n ;
- $\mathbf{z}[n]$ is a size- N_r vector of zero-mean, circularly-invariant Gaussian-noise samples, with variance σ^2 per real dimension, which are assumed to be independent across time and for each receive antenna.

For the phase-noise samples, time dependency is kept into account by assuming Wiener phase-noise processes:

$$\phi_i[n] = \phi_i[n-1] + w_i[n], \quad i = 1, \dots, O_r + O_t, \quad n = 1, 2, \dots \quad (2)$$

where $\phi_1[0], \dots, \phi_{O_r+O_t}[0]$ are independent and uniformly distributed in $[0, 2\pi)$, and $w_1[n], \dots, w_{O_r+O_t}[n]$

are independent zero-mean white Gaussian processes with power ρ^2 (all processes have the same power).

Before describing the proposed detector, let us notice that each tap of the MIMO channel is affected by the sum of one transmit and one receive phase-noise process. We define a *sum* phase-noise process as:

$$\phi_{ii'}[n] = \phi_i[n] + \phi_{O_t+i'}[n], \quad i = 1, \dots, O_t, \quad i' = 1, \dots, O_r. \quad (3)$$

Unlike the $\phi_i[n]$ processes, which will be called *atomic* hereafter, two sum phase-noise processes are correlated if they share one index. Moreover, they can all be written as linear functions of $\phi_{i1}[n]$, $i = 1, \dots, O_t$ and $\phi_{1i'}[n]$, $i' = 2, \dots, O_r$, as:

$$\phi_{ii'}[n] = \phi_{i1}[n] + \phi_{1i'}[n] - \phi_{11}[n]. \quad (4)$$

Thus, the whole set of $O_r O_t$ sum phase-noise processes is generated from a basis with $O_r + O_t - 1$ elements. Although atomic phase-noise processes have a simpler statistical characterization, they are not observable, so that phase estimation must pass through sum phase-noise process estimation.

We define for future use the size- $(O_t + O_r)$ vector $\phi[n]$, whose i -th element is $\phi_i[n]$, $i = 1, \dots, O_r + O_t$. Analogously, we define the size- $(O_t O_r)$ vector $\phi^{\text{sum}}[n]$, whose element $(i - 1)O_r + i'$ is $\phi_{ii'}[n]$, $i = 1, \dots, O_t$, $i' = 1, \dots, O_r$.

B. Pilot transmission scheme and channel estimation

The underlying hypothesis behind the channel model in (1) is that the channel matrix $\mathbf{H}[n]$ changes in time much more slowly than the PN. Thus, channel estimation can be performed less frequently than phase detection. In particular, we will suppose that there are two kinds of pilots in the system, with the first pilot type devoted to joint channel and phase estimation (as it is not possible, in principle, to distinguish the phase of unknown channel matrix entries from PN), and the second devoted only to phase detection.

The first type of pilots, called hereafter channel pilots, will be transmitted during N_t consecutive channel uses, after which a frame of L channel uses begins. The average energy of channel pilots will be denoted E_C . The overall average energy of transmitted symbols will then be²

$$\overline{E} = \frac{L}{L + N_t} E_s + \frac{N_t}{L + N_t} E_C. \quad (6)$$

²If we consider single-antenna users, then the average transmitted symbol energy *per user* will be

$$\overline{E} = \frac{L}{L + N_t} E_s + \frac{1}{L + N_t} E_C. \quad (5)$$

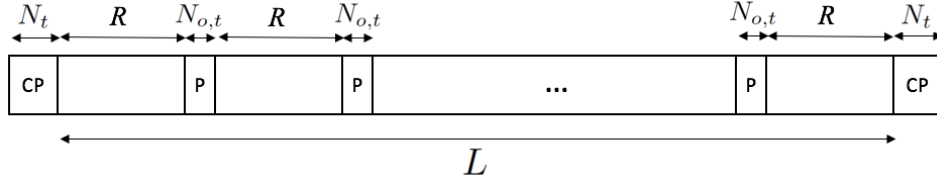


Fig. 2. Frame structure for the proposed massive MIMO transmission scheme. CP: channel estimation pilots. P: phase-noise estimation pilots.

During such frame, we will make the assumption that the channel matrix stays constant (corresponding to a non-fading or block fading scenario), so that we will write simply \mathbf{H} instead of $\mathbf{H}[n]$. Moreover, different frames are treated independently, so that, for our purposes, we can consider a single frame, where channel estimation is performed at the beginning, say at step 0. As a result of channel estimation, the receiver will obtain a noisy version of \mathbf{H} , i.e.,³

$$\hat{\mathbf{H}} = \Phi_R[0] \mathbf{H} \Phi_T[0] + \mathbf{Z}_C, \quad (7)$$

where \mathbf{Z}_C is the channel estimation error, assumed to be composed of i.i.d. zero-mean Gaussian RV's with variance σ^2/E_C per real dimension. In our model, we can always embed the initial phase-noise values into the channel matrix and assume that the phase-noise processes start from zero, or, equivalently, that we estimate differential processes $\phi_i[n] - \phi_i[0]$, $i = 1, \dots, O_r + O_t$. With this in mind, we can redefine the channel matrix to be

$$\tilde{\mathbf{H}} = \hat{\mathbf{H}} + \tilde{\mathbf{Z}}_C, \quad (8)$$

where $\tilde{\mathbf{H}} = \Phi_R[0] \mathbf{H} \Phi_T[0]$ and $\tilde{\mathbf{Z}}_C = -\mathbf{Z}_C \sim \mathcal{N}(\mathbf{0}, \frac{\sigma^2}{E_C} \mathbf{I}_{N_r})$.

The second type of pilots, used within the frame only to perform coarse phase detection, consists of $N_{o,t}$ orthogonal pilots, after which a block of R data symbol vectors are transmitted. Such phase pilots are used to obtain a rough estimate of sum phase-noise processes at pilot positions, after which MMSE filtering is performed to yield an estimate of *atomic* phase-noise processes. Finally, linear interpolation allows to obtain an initial phase estimate also for data positions, which will constitute a starting point for the EM-based receiver described in the next subsection. For more details on the EM initialization, see [4]. For clarity, in Fig. 2, we have depicted the structure of the frame with the diverse pilot and data transmission intervals.

³Here, we assume implicitly that PN stays constant during the channel estimation phase.

III. THE EM-BASED RECEIVER

Suppose the information transmitted by the k -th user, $k = 1, \dots, K$, is encoded with a channel encoder. The codeword is then mapped to a stream of QAM symbols, belonging to an M -size constellation $\{\mathbf{x}^{(p)}\}_{p=1}^M$, and transmitted to the BS. Let us collect all symbols transmitted by all users into a frame of L symbol vectors $\mathbf{X} = (\mathbf{x}[1], \dots, \mathbf{x}[L])$. Each symbol vector is transmitted through the channel described by equation (1). The channel output in a frame is then collected in the matrix $\mathbf{Y} = (\mathbf{y}[1], \dots, \mathbf{y}[L])$.

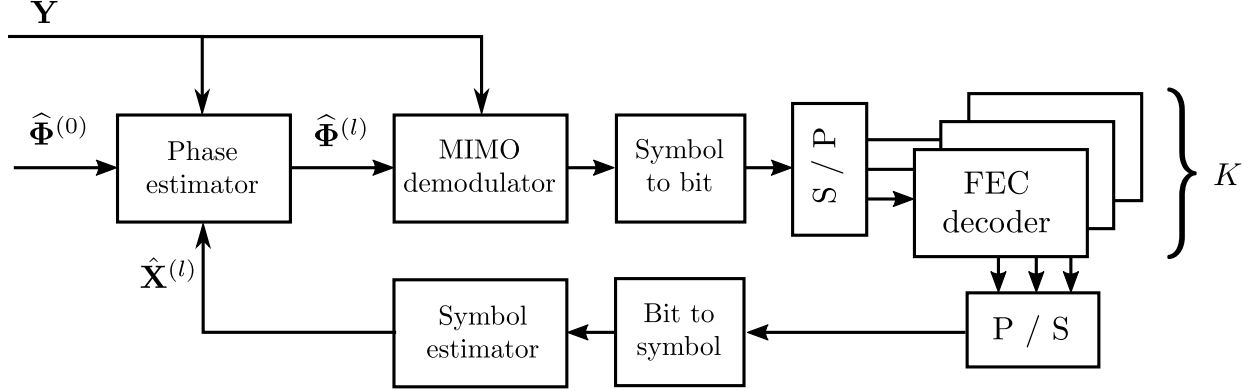


Fig. 3. Structure of the iterative receiver.

The EM-based receiver here described is an iterative approximation of joint phase detection and demodulation. The block diagram can be seen in Fig. 3. Starting from an initial pilot-based phase estimate $\hat{\Phi}^{(0)}$, the receiver obtains at the l -th iteration the phase estimate $\hat{\Phi}^{(l)}$. The latter is then used in the MIMO demodulator to compute log-likelihood ratios (LLRs) for the transmitted symbols. These are converted to bit LLRs and input to the FEC decoders, one for each user. The decoders' output is then mapped into estimated transmitted symbols $\hat{\mathbf{X}}^{(l)}$ and fed back to the phase estimator for the subsequent $(l + 1)$ -th iteration. In the first iteration, there is no prior information about estimated received symbols. In Subsection III-A, we will explain in detail the phase estimation algorithm, while in Subsection III-B we briefly describe the MIMO demodulator.

A. Phase estimator

Before proceeding further, we have to define some notation. We will denote with $\tilde{\mathbf{H}}_{ij}$, $i = 1, \dots, O_r$, $j = 1, \dots, O_t$, the $N_{o,r} \times N_{o,t}$ block of $\tilde{\mathbf{H}}$ corresponding to oscillators j and $O_t + i$ at the transmitter and receiver side, respectively. Moreover, $\tilde{\mathbf{H}}_i$, $i = 1, \dots, O_t$ will be the $N_r \times N_{o,t}$ matrix obtained by stacking all matrices $\tilde{\mathbf{H}}_{ji}$ for $j = 1, \dots, O_r$. Finally, we will denote with $\tilde{\mathbf{H}}_{O_t+i}$, $i = 1, \dots, O_r$ the $N_{o,r} \times N_t$ matrix

obtained by juxtaposing all matrices $\widehat{\mathbf{H}}_{ij}$ for $j = 1, \dots, O_t$. With $\widehat{\mathbf{H}}_{ij}$, $\widehat{\mathbf{H}}_i$ and $\widehat{\mathbf{H}}_{O_t+i}$ we will denote the corresponding estimated submatrices.

Let us define $f_A(\Phi)$ as the a priori distribution of $\Phi = (\phi[1], \dots, \phi[L])$. The goal of the phase detection stage is to obtain the maximum a posteriori estimate of Φ , i.e.,

$$\begin{aligned} \widehat{\Phi} &= (\widehat{\phi}[1], \dots, \widehat{\phi}[L]) \\ &= \arg \max_{\Phi} \left(E_{\mathbf{X}} \prod_{n=1}^L \Pr \{ \mathbf{y}[n] | \mathbf{x}[n], \phi[n] \} f_A(\Phi) \right). \end{aligned} \quad (9)$$

Since the computation of $\widehat{\Phi}$ cannot be performed analytically for a Wiener phase-noise process, the EM algorithm is a way to approach iteratively the solution of (9), starting from an initial estimate $\widehat{\Phi}^{(0)}$, by ideally applying at iteration l , $l = 1, 2, \dots$, the following two steps.

E step: Given $\widehat{\Phi}^{(l-1)}$, the average over the transmitted symbols should be computed as follows:

$$h^{(l)}(\Phi) = E_{\mathbf{X}}^{(l)} \log \prod_{n=1}^L \Pr \{ \mathbf{y}[n] | \mathbf{x}[n], \phi[n] \}, \quad (10)$$

where the average is performed according to the distribution $\Pr\{\mathbf{X} | \mathbf{Y}, \widehat{\Phi}^{(l-1)}\}$.

M step: The following maximization problem should be solved:

$$\widehat{\Phi}^{(l)} = \arg \max_{\Phi} (h^{(l)}(\Phi) + \log f_A(\Phi)). \quad (11)$$

For the channel model in (1), apart from an inessential additive constant, (10) becomes:

$$h^{(l)}(\Phi) = E_{\mathbf{X}}^{(l)} \sum_{n=1}^L \frac{\Re\{ \mathbf{x}^H[n] \Phi_T^H[n] \widehat{\mathbf{H}}^H \Phi_R^H[n] \mathbf{y}[n] \} - \frac{1}{2} \|\widehat{\mathbf{H}} \Phi_T[n] \mathbf{x}[n]\|^2}{\sigma^2 (1 + E_C^{-1} \mathbf{x}^H[n] \mathbf{x}[n])}, \quad (12)$$

where the two terms in the denominator account for both the additive white Gaussian noise and the noisy channel estimation. It is shown in [4] that there is no substantial performance loss if we substitute the average on \mathbf{X} with the hard estimate of the transmitted symbols at iteration l , which we denote as $\widehat{\mathbf{X}}^{(l)} = (\widehat{\mathbf{x}}^{(l)}[1], \dots, \widehat{\mathbf{x}}^{(l)}[L])$. Thus, we make the following approximation:

$$h^{(l)}(\Phi) \simeq \sum_{n=1}^L \frac{\Re\{ (\widehat{\mathbf{x}}^{(l)}[n])^H \Phi_T^H[n] \widehat{\mathbf{H}}^H \Phi_R^H[n] \mathbf{y}[n] \} - \frac{1}{2} \|\widehat{\mathbf{H}} \Phi_T[n] \widehat{\mathbf{x}}^{(l)}[n]\|^2}{\sigma^2 (1 + E_C^{-1} (\widehat{\mathbf{x}}^{(l)}[n])^H \widehat{\mathbf{x}}^{(l)}[n])}. \quad (13)$$

In practice, as in [23], the maximization involved in the M step is approximated through the steepest-descent algorithm, and only the gradient of function $h^{(l)}(\Phi)$ is computed in the phase estimator. Let $\widehat{\Phi}_m^{(l)}$

be the estimate of $\widehat{\Phi}^{(l)}$ after m steepest-descent iterations (starting from $\widehat{\Phi}_0^{(l)} = \widehat{\Phi}^{(0)}$). Then:

$$\widehat{\Phi}_m^{(l)} = \widehat{\Phi}_{m-1}^{(l)} + \lambda_m^{(l)} \nabla_{\Phi} \left(h^{(l)}(\Phi) + \log f_A(\Phi) \right) \Big|_{\widehat{\Phi}_{m-1}^{(l)}}, \quad (14)$$

where $\lambda_m^{(l)}$ is the m -th step size of the steepest-descent algorithm at iteration l . The derivative of $h^{(l)}(\Phi)$ with respect to $\phi_i[n]$, $i = 1, \dots, O_t$, is readily computed as:

$$\frac{\partial}{\partial \phi_i[n]} h^{(l)}(\Phi) \simeq \frac{\Im \{ e^{-j\phi_i[n]} (\widehat{\mathbf{x}}_i^{(l)}[n])^H \widehat{\mathbf{H}}_i^H (\Phi_R^H[n] \mathbf{y}[n] - \widehat{\mathbf{H}} \Phi_T[n] \widehat{\mathbf{x}}^{(l)}[n]) \}}{\sigma^2 (1 + E_C^{-1} (\widehat{\mathbf{x}}^{(l)}[n])^H \widehat{\mathbf{x}}^{(l)}[n])}, \quad (15)$$

with $\widehat{\mathbf{x}}_i^{(l)}[n]$ the length- $N_{o,t}$ subvector of $\widehat{\mathbf{x}}^{(l)}[n]$ corresponding to transmit oscillator i . Analogously, the derivative of $h^{(l)}(\Phi)$ with respect to $\phi_{O_t+i}[n]$, $i = 1, \dots, O_r$, results:

$$\frac{\partial}{\partial \phi_{O_t+i}[n]} h^{(l)}(\Phi) \simeq \frac{\Im \{ e^{-j\phi_{O_t+i}[n]} (\widehat{\mathbf{x}}^{(l)}[n])^H \Phi_T^H[n] \widehat{\mathbf{H}}_{O_t+i}^H \mathbf{y}_i[n] \}}{\sigma^2 (1 + E_C^{-1} (\widehat{\mathbf{x}}^{(l)}[n])^H \widehat{\mathbf{x}}^{(l)}[n])}, \quad (16)$$

with $\mathbf{y}_i[n]$ the length- $N_{o,r}$ subvector of $\mathbf{y}[n]$ corresponding to receiver oscillator $O_t + i$. Moreover, thanks to the Wiener model, we have (with a slight abuse of notation):

$$\log f_A(\Phi) = \log f_A(\phi[0]) + \sum_{n=1}^L \log f_A(\phi[n+1]|\phi[n]), \quad (17)$$

so that, provided that $\rho^2 \ll 2\pi$ (a usually realistic approximation), we obtain [23]:

$$\begin{aligned} \frac{\partial}{\partial \phi_i[n]} \log f_A(\Phi) &= \frac{\partial}{\partial \phi_i[n]} \log f_A(\phi[n]|\phi[n-1]) + \\ &\quad \frac{\partial}{\partial \phi_i[n]} \log f_A(\phi[n+1]|\phi[n]) \\ &\simeq \frac{\phi_i[n-1] - \phi_i[n] + k_{n-1}2\pi}{\rho^2} + \\ &\quad \frac{\phi_i[n+1] - \phi_i[n] + k_n2\pi}{\rho^2}, \end{aligned} \quad (18)$$

where k_n and k_{n-1} are signed integers that minimize the moduli of the numerators.

1) *Step size optimization and stopping rule:* In order to improve the convergence of the steepest-descent algorithm, we have dynamically chosen the step size $\lambda_m^{(l)}$ as follows.

- In the first step ($m = 1$), we adopt the backtracking line search approach. Namely, we start from a maximum candidate value for $\lambda_1^{(l)}$, and we progressively reduce it until Armijo's condition is satisfied [24], i.e.

$$g \left(\widehat{\Phi}_0^{(l)} + \lambda_1^{(l)} \nabla g \left(\widehat{\Phi}_0^{(l)} \right) \right) \geq g \left(\widehat{\Phi}_0^{(l)} \right) + \lambda_1^{(l)} c \left\| \nabla g \left(\widehat{\Phi}_0^{(l)} \right) \right\|^2, \quad (19)$$

where $g(\Phi) = (h^{(l)}(\Phi) + \log f_A(\Phi))$ and c is a constant, set to $c = 0.5$ in our simulations. The progressive reduction of $\lambda_1^{(l)}$ from the initial value is performed with steps of 0.5.

- In the subsequent iterations ($m > 1$), we use the Barzilai-Borwein method to set the step size [25], yielding:

$$\lambda_m^{(l)} = \frac{\left| \left(\widehat{\Phi}_{m-1}^{(l)} - \widehat{\Phi}_{m-2}^{(l)} \right)^T \cdot \left(\nabla g \left(\widehat{\Phi}_{m-1}^{(l)} \right) - \nabla g \left(\widehat{\Phi}_{m-2}^{(l)} \right) \right) \right|}{\left\| \nabla g \left(\widehat{\Phi}_{m-1}^{(l)} \right) - \nabla g \left(\widehat{\Phi}_{m-2}^{(l)} \right) \right\|^2}. \quad (20)$$

The steepest-descent iterations are stopped whenever the increment in the objective function falls beyond a given threshold, i.e., whenever

$$\frac{\left| g \left(\widehat{\Phi}_m^{(l)} \right) - g \left(\widehat{\Phi}_{m-1}^{(l)} \right) \right|}{g \left(\widehat{\Phi}_{m-1}^{(l)} \right)} < \theta. \quad (21)$$

Setting an appropriate value for θ requires meeting a trade-off between convergence time and final error performance, as will be shown in Section V.

B. MIMO demodulator

At a given receiver iteration, the block labelled ‘‘MIMO demodulator’’ in Fig. 3 derives LLRs on symbols, based on the current phase-noise estimates, followed by a standard extraction of LLRs on coded bits. These bit LLRs are then input to the channel decoder. Due to the large size of the massive MIMO system, we propose a suboptimal MIMO demodulator, based on linear minimum mean-square error (LMMSE) filtering. Explicitly, at iteration l and channel use n , symbol LLRs are computed on a per-symbol basis from the LMMSE filter output

$$\tilde{\mathbf{y}}[n] = \mathbf{F}^{(l)}[n]\mathbf{y}[n], \quad (22)$$

where

$$\mathbf{F}^{(l)}[n] = \left(\widehat{\mathbf{H}}^H \widehat{\mathbf{H}} + \sigma^2 \left(\frac{N_t}{E_C} + \frac{1}{E_s} \right) \right)^{-1} \widehat{\mathbf{H}}^H. \quad (23)$$

Notice that the above filter expression takes into account the effect of imperfect CSI.

IV. BAYESIAN CRAMER-RAO BOUND

In this section, we compute the BCRB for the system described in the previous section, under the hypothesis that the transmitted symbols are *known* at the receiver and assuming perfect channel state information. This hypothesis suits well the case of the EM receiver, since, if convergence eventually

occurs, the output of the channel decoder after several iterations provides the phase detector with (almost) perfect knowledge of the transmitted symbols. The subject of this subsection is the generalization of the BCRB computation in [26], [27], which considers the particular case of $N_{o,t} = N_{o,r} = 1$.

The BCRB allows to lower-bound the MSE between the unknown phase-noise sample sequence and its estimate performed by the phase detector at the receiver. Let $\bar{\phi}^{\text{sum}}$ be the size- $O_t O_r L$ column vector obtained by stacking all vectors $\phi^{\text{sum}}[1], \dots, \phi^{\text{sum}}[L]$ and let $\hat{\phi}^{\text{sum}}$ be any possible estimate of $\bar{\phi}^{\text{sum}}$. The covariance matrix Σ of such estimate is given by

$$\Sigma = \mathbb{E}_{\Phi, \mathbf{Y}, \mathbf{X}, \hat{\mathbf{H}}} \left\{ \left(\hat{\phi}^{\text{sum}} - \bar{\phi}^{\text{sum}} \right) \cdot \left(\hat{\phi}^{\text{sum}} - \bar{\phi}^{\text{sum}} \right)^{\text{T}} \right\}. \quad (24)$$

The BCRB then states that

$$\Sigma \succeq \mathbf{M}^{-1}, \quad (25)$$

where \mathbf{M} is the Bayesian information matrix (BIM) defined by

$$\mathbf{M} = -\mathbb{E}_{\Phi, \mathbf{Y}, \mathbf{X}} \left\{ \nabla_{\bar{\phi}^{\text{sum}}} \nabla_{\bar{\phi}^{\text{sum}}}^{\text{T}} \log f(\mathbf{Y}, \bar{\phi}^{\text{sum}} | \mathbf{X}) \right\}. \quad (26)$$

Conditioning on \mathbf{X} in the above definition corresponds to the hypothesis of known transmitted symbols. Considering the i -th element of vector $\bar{\phi}^{\text{sum}}$, the BCRB implies that:

$$(\Sigma)_{i,i} \geq (\mathbf{M}^{-1})_{i,i}, \quad (27)$$

i.e., the BCRB provides lower bounds to the MSE for every estimator of the sum phase-noise samples.

The result is summarized in the following proposition.

Proposition 1: For the channel model in (1), if $\rho \ll 2\pi$, the BIM \mathbf{M} defined in (26) is given by

$$\mathbf{M} = \begin{bmatrix} \mathbf{M}_0 & \mathbf{M}_1 & & & \\ \mathbf{M}_1 & \mathbf{M}_0 & \mathbf{M}_1 & & \\ & \mathbf{M}_1 & \mathbf{M}_0 & \ddots & \\ & & \ddots & \ddots & \mathbf{M}_1 \\ & & & \mathbf{M}_1 & \mathbf{M}_0 \end{bmatrix}, \quad (28)$$

where $\mathbf{M}_0 = \mathbf{J}^{\text{T}} \widetilde{\mathbf{M}}_0 \mathbf{J}$ and $\mathbf{M}_1 = \mathbf{J}^{\text{T}} \widetilde{\mathbf{M}}_1 \mathbf{J}$, \mathbf{J} being the Jacobian of the transformation from sum processes

to atomic processes at a given time n , $\widetilde{\mathbf{M}}_1 = -\frac{1}{\rho^2}\mathbf{I}_{O_t+O_r}$ and $\widetilde{\mathbf{M}}_0 = \widetilde{\mathbf{M}}_0^Y + \frac{2}{\rho^2}\mathbf{I}_{O_t+O_r}$, and

$$\widetilde{\mathbf{M}}_0^Y = \frac{1}{\sigma^2} \begin{bmatrix} \mathbf{\Gamma}_T & \mathbf{\Omega}^\top \\ \mathbf{\Omega} & \mathbf{\Gamma}_R \end{bmatrix}, \quad (29)$$

where

$$\mathbf{\Gamma}_T = \text{diag}(\|\mathbf{H}_1\|_F^2, \dots, \|\mathbf{H}_{O_t}\|_F^2)$$

$$\mathbf{\Gamma}_R = \text{diag}(\|\mathbf{H}_{O_t+1}\|_F^2, \dots, \|\mathbf{H}_{O_t+O_r}\|_F^2),$$

and $\mathbf{\Omega}$ an $O_r \times O_t$ matrix whose (i, j) entry is given by

$$\Omega_{ij} = \|\mathbf{H}_{ij}\|_F^2.$$

Proof: The formula is a rather straightforward generalization of those in [26], [27]. ■

V. SIMULATION RESULTS

In this section, we present comparative simulation results for some meaningful test cases. These have been performed for a scenario under the following specific conditions:

- The modulation chosen is 64-QAM, with efficiency 6 bits per symbol.
- The FEC scheme chosen is the 5G NR LDPC code of type 2 and lift factor $Z = 2$, with a length $N = 104$ bits and a rate equal to 0.8 [28]. The number of LDPC decoding iterations is set to 50.
- The PN standard deviation is $\rho = 0.2$ radians.
- In general, we consider a Rice-fading channel matrix given by

$$\mathbf{H} = \sqrt{\frac{K_{Rice}}{K_{Rice} + 1}} \mathbf{H}_{\text{LOS}} + \sqrt{\frac{1}{K_{Rice} + 1}} \mathbf{H}_w \quad (30)$$

where \mathbf{H}_w is composed by i.i.d. zero-mean circular complex Gaussian RV's and \mathbf{H}_{LOS} is composed by unit-modulus entries with i.i.d. phases uniformly distributed in $[0, 2\pi)$. Unless otherwise stated, we set $K_{Rice} = 100$ dB, so that $\mathbf{H} = \mathbf{H}_{\text{LOS}}$.

- In the case of the simulations run to get BER statistics, a genie-aided decoding stopping rule is activated, in order to speed up the process. No such rule is activated in the case of the simulations run to get MSE statistics.
- The frame length takes value $L = 1086$ symbols.

- The channel coherence time is L symbol periods (block fading).
- At the transmitter side $K = O_t = 16$. Moreover, since we are considering an uplink massive MIMO for mobile communications, $N_{o,t}$ would be set to 2 (two antennas for each user).
- At the receiver side, we set $N_r = 64$, with $O_r = 4$ (four oscillators at the RX side, feeding $N_{o,r} = 16$ antennas each).
- Unless otherwise stated, the maximum number of receiver iterations is set to 10.
- Each frame is built to contain 1000 LDPC codewords.
- The simulations to obtain the BER results have been obtained for up to 100 frames in error, with a maximum number of 10^6 simulated frames.
- The maximum number of iterations in the steepest-descent algorithm has been set to 300.

A. MSE simulation results

Figs. 4-6 show the MSE of the phase estimation and the corresponding BCRB for several setups.

In Fig. 4, the curves show the MSE for different number of receiver iterations and several choices of the threshold θ to stop steepest-descent steps, as per (21). The red curve shows the MSE for $\theta = 10^{-6}$ and 10 receiver iterations. The benefit of the iterative receiver can be observed by comparing such curve with the green one, which corresponds to the MSE performance after one receiver iteration. Since the green curve has a lower slope, the benefit increases with the SNR, reaching about 7 dB for $\text{MSE} = 2 \times 10^{-4}$. However, most of the gain is obtained already at the second iteration, as shown by the black curve, which is essentially superimposed to the red curve. The magenta curve shows the MSE performance for $\theta = 10^{-7}$ and 10 receiver iterations. The gain with respect to the red curve ranges from 2 to 5 dB but the slope of the two curves is about the same. However, as it will be evident from the results in Subsection V-B, when $\theta = 10^{-7}$, the average total number of steepest-descent steps is larger than for $\theta = 10^{-6}$, being for example 1240 for the former case and 741 for the latter at $E_s/N_0 = 9$ dB. At an SNR large enough, the curves for 10 iterations are essentially parallel to the BCRB, with an SNR gap at $\text{MSE} = 10^{-4}$ of about 10 dB for $\theta = 10^{-6}$ and 5 dB for $\theta = 10^{-7}$.

In the following, for all simulation results, we have set a threshold $\theta = 10^{-6}$ and 10 receiver iterations. In Fig. 5, we show the effect of imperfect channel CSI. The red curve shows the performance for perfect CSI (same as in Fig. 4). The other curves show the performance with imperfect CSI and different channel pilot power. In particular, taking into account that E_C is the energy of channel pilots, the curves from top to bottom correspond to a ratio E_C/E_s equal to 5, 10, 15 and 20 dB, respectively. As it can be seen,

the green curve is heavily affected at low-to-medium SNR values by the channel uncertainty. The black curve, which is obtained by supposing a power for pilots 10 times the power for payload, loses 5-6 dB with respect to perfect CSI, for $\text{MSE} < 3 \times 10^{-4}$.

Fig. 5 shows the effect of fading. The different curves are obtained with different values of the Rice factor, ranging from $K_{Rice} = 100$ dB, i.e., pure LOS, to $K_{Rice} = -100$ dB, i.e., Rayleigh fading. As it can be seen, above an SNR of 10 dB, the MSE curves are only marginally affected by the fading amount, with the MSE slightly increasing with decreasing K_{Rice} . It is worth noting that the BCRB is virtually independent of K_{Rice} , since, due to the large MIMO size and to the expression of the BIM in (28), an average effect takes place.

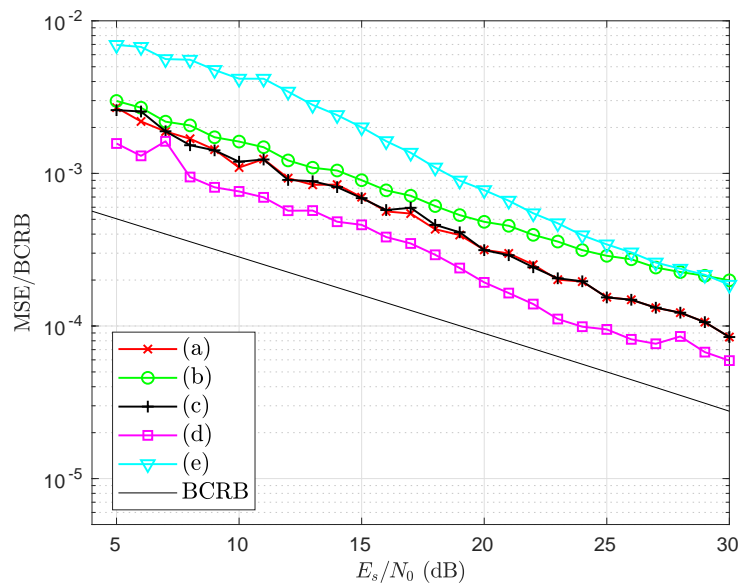


Fig. 4. MSE results for perfect CSI. (a) Threshold $\theta = 10^{-6}$ and 10 receiver iterations. (b) Threshold $\theta = 10^{-6}$ and 1 receiver iteration. (c) Threshold $\theta = 10^{-6}$ and 2 receiver iterations. (d) Threshold $\theta = 10^{-7}$ and 10 receiver iterations. (e) Threshold $\theta = 10^{-4}$ and 10 receiver iterations.

B. BER simulation results

In Figs. 7 to 9, we have depicted the BER results for various parameters, keeping the number of antennas and oscillators of the basic setup used to illustrate the MSE behavior.

In Fig. 7, we show the impact of PN on the system BER. First of all, the red curve depicts the BER for the case in which the PN has power $\rho = 0.2$ and there is no phase detection. As it can be seen, the curve gets flatter and flatter as the SNR increases, since for high SNR PN becomes a major source of disturbance. If we employ a non-iterative receiver that performs phase estimation as described in the previous sections, the BER performance gets much better, as the black curve shows. It is somehow surprising that the BER

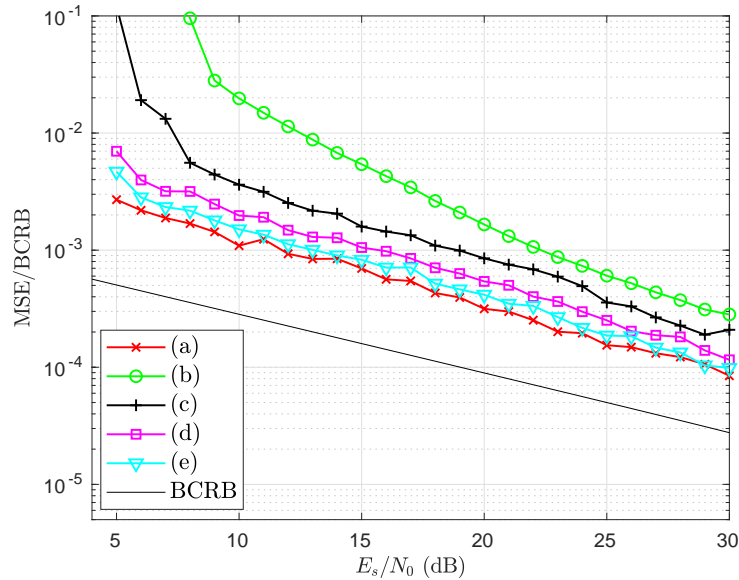


Fig. 5. MSE results for perfect and non-perfect CSI. In all the cases, $\theta = 10^{-6}$ and we have performed 10 receiver iterations. (a) Perfect CSI. (b) $E_C/E_s = 5$ dB. (c) $E_C/E_s = 10$ dB. (d) $E_C/E_s = 15$ dB. (e) $E_C/E_s = 20$ dB.

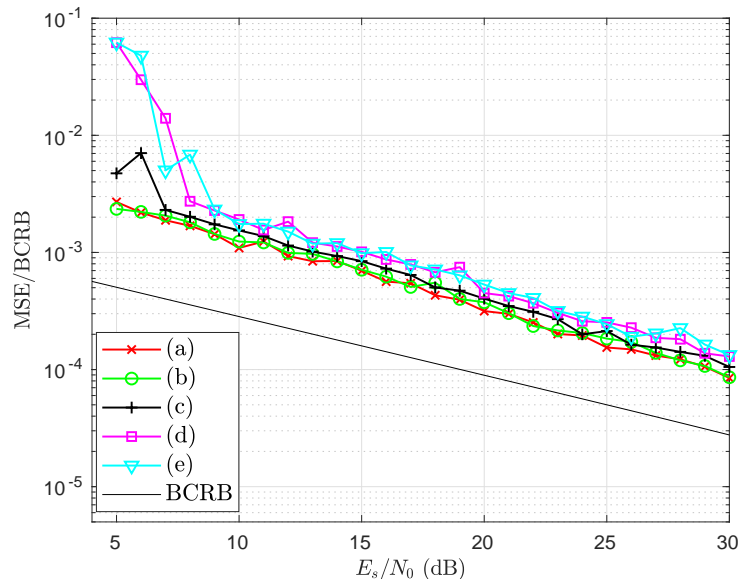


Fig. 6. MSE results for the fading channel. BCRB is the same for AWGN and for every K_{Rice} factor. In all the cases, $\theta = 10^{-6}$ and we have performed 10 receiver iterations (a) $K_{Rice} = 100$ dB. (b) $K_{Rice} = 10$ dB. (c) $K_{Rice} = 0$ dB. (d) $K_{Rice} = -10$ dB. (e) $K_{Rice} = -100$ dB.

is only slightly worse than in the case without PN (green curve), specially after 15 dB, in correspondence with what was shown in Fig. 4, where the MSE slope starts diverging from the BCRB trend. But the major improvement comes in with iterations, as shown by the light-blue curve, which corresponds to a maximum number of 10 iterations. Once again, the proposed receiver is able to virtually achieve the BER of the case without PN, with the same number of iterations. The receiver without PN takes advantage of

the iterations in the MIMO demodulator and in the symbol-to-bit demapper. Finally, if we increase the PN power to $\rho = 1.0$, the performance loss is negligible, as clearly seen by the dark-blue curve.

From now on, we set $\rho = 0.2$ and up to 10 receiver iterations. In Fig. 8, we show the effect on BER of imperfect CSI. Like in Fig. 5, we consider different relative power levels for channel pilots. For $BER = 10^{-4}$, $E_C/E_s = 5$ dB (green curve) entails a 11-dB loss with respect to the perfect-CSI case, while $E_C/E_s = 10$ dB (black curve) reduces the loss to about 8 dB. Allowing $E_C/E_s = 20$ dB (light-blue curve) is able to yield a limited loss of about 1.5 dB. These gaps are in good accordance with those for MSE, as can be stated from Figure 5.

In Fig. 9, we depict the results with perfect CSI but different K_{Rice} values, displaying the same cases as in Fig. 6. As it can be verified, for a given performance, we have SNR differences very close to those shown in Fig. 6 respecting the MSE. For example, for a BER of 10^{-4} , we can see the SNR gap between $K_{Rice} = 100$ dB and $K_{Rice} = 10$ dB is less than half a dB. The same happens if we consider $K_{Rice} = -10$ dB and $K_{Rice} = -100$ dB. For $K_{Rice} = 0$ dB, the SNR needed to attain said target BER value lies between 1 dB and 2 dB apart with respect to the cases with $K_{Rice} = 10$ dB and $K_{Rice} = -10$ dB. This is fully consistent with the differences in SNR we can appreciate in Fig. 6 for an MSE of 10^{-3} , for example.

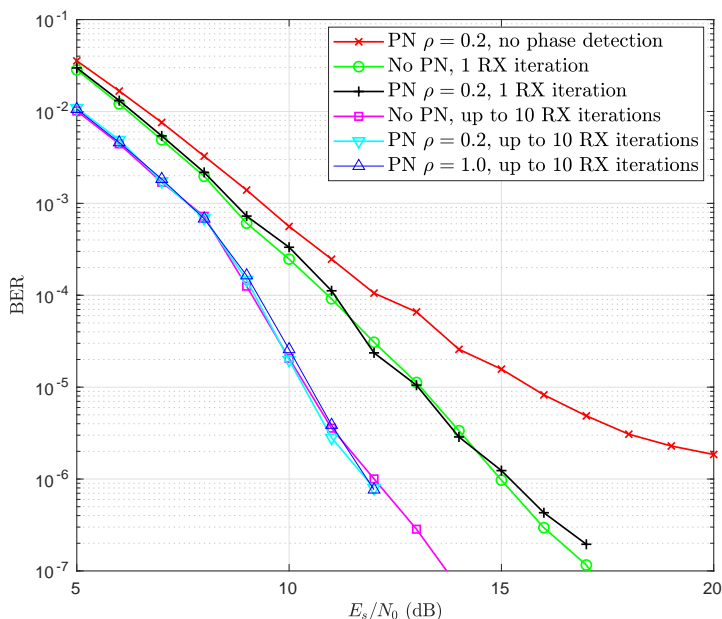


Fig. 7. BER results for different cases with or without added PN (cases PN vs. No PN), and several receiver strategies (including no phase detection and a variable maximum number of iterations).

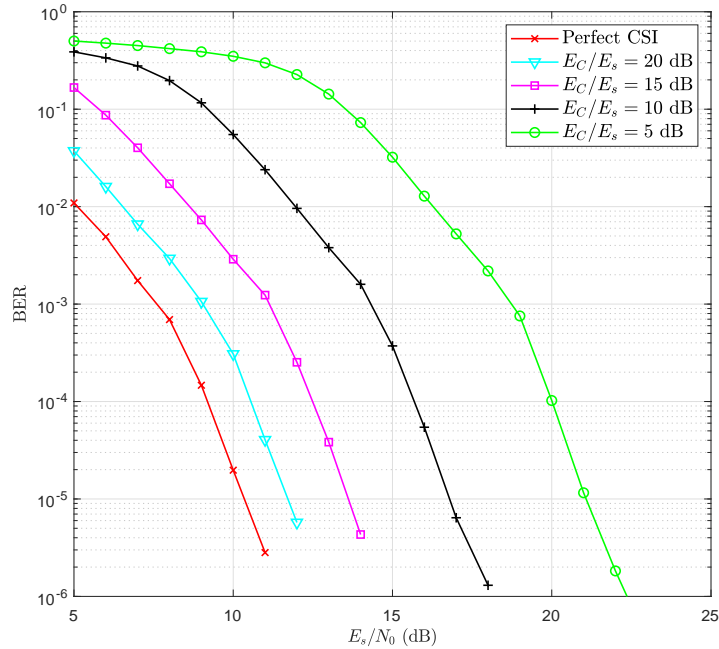


Fig. 8. BER results for different cases with perfect and non-perfect CSI. In all the cases, the maximum number of receiver iterations is 10, and the threshold for the steepest-descent algorithm is $\theta = 10^{-6}$.

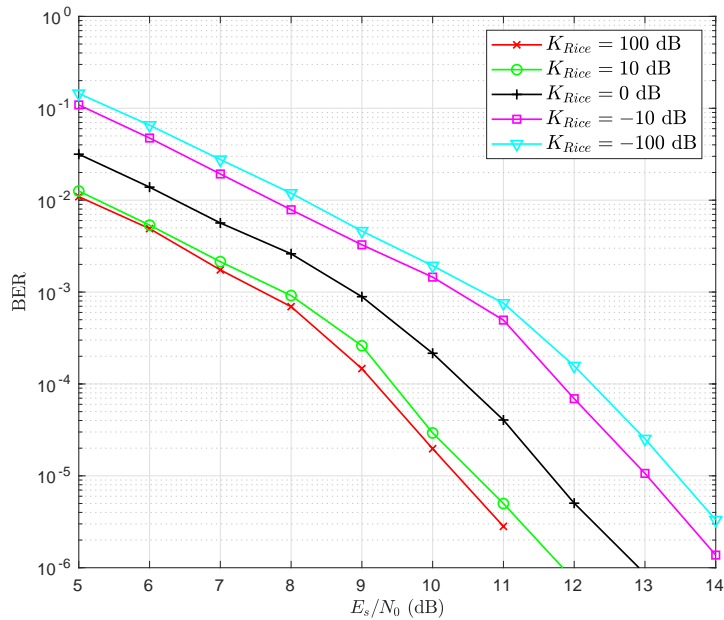


Fig. 9. BER results for the fading channel, with K_{Rice} ranging from 100 to -100 dB. In all the cases, the maximum number of receiver iterations is 10, and the threshold for the steepest-descent algorithm is $\theta = 10^{-6}$.

C. Average number of receiver iterations and steepest-descent steps

In Fig. 10, we represent the average number of receiver iterations performed as a function of the SNR, in the nominal case (no fading, perfect CSI), for different thresholds θ , and in Fig. 11 we depict the average

total number of steepest-descent steps required. These figures allow understanding the computational requirements for the phase detection and correction process in each case, and may help in establishing important trade-offs. Fig. 10 shows how the threshold for the steepest-descent algorithm does not seem to affect much the average number of receiver iterations required to trigger the stopping rule as a function of the SNR. In general, we may distinguish three zones in the plots: for low SNR, the maximum number of receiver iterations (up to 10) is performed because the stopping rule is not triggered; for an SNR range between roughly 7 and 11 dB, we have a steep descent in the number of iterations, a fact which is coherent with the activation of the stopping rule and the progressively better performance of the phase detection algorithm and the decoding step; finally, for large SNR (from 12 dB and on), we reach a floor where basically only one receiver iteration is performed, though from time to time up to two iterations would be performed in given cases and the average does not strictly fall to 1 iteration. It is to be noted that, in the transition zone, there is a slight difference as a function of the threshold θ (for example, at 9 dB): a case with a higher threshold (i.e., $\theta = 10^{-4}$) requires an average number of iterations slightly higher than for lower values, and there is a consistent trend with decreasing θ . This is logical, given that a lower threshold will provide a lower MSE (see Fig. 4) and the stopping rule will be triggered earlier.

Respecting Fig. 11, we can see a picture of how the steepest-descent algorithm performs throughout the detection process. We depict the *average total number* of steepest-descent steps for the same setup as in Fig. 10: it is the total throughout all the receiver iterations, and it is an average respecting the number of frames processed. As it may be seen, and in contrast with Fig. 10, there is always a non vanishing difference among the different thresholds, since, for a lower θ , the algorithm will perform more steepest-descent steps regardless of the SNR level. In any case, the differences are higher for low SNR values (where a large amount of receiver iterations have to be performed), while, after the descent from 7 to 11 dB (which also reflects the trend identified in Fig. 10), each case seems to stabilize around a value which decreases with higher values of θ , as expected.

Though not shown, the BER results are basically the same for $\theta = 10^{-7}$ and $\theta = 10^{-6}$, while they slightly degrade for $\theta = 10^{-5}$ and $\theta = 10^{-4}$. This fact, together with the information provided by Figs. 10 and 11, helps to identify as a convenient trade-off threshold value $\theta = 10^{-6}$: it keeps the complexity as low as possible without noticeable BER degradation. It is worth noting that, for $\theta = 10^{-6}$, the MSE is slightly worse with respect to the $\theta = 10^{-7}$ case: this seeming contradiction probably arises from the fact that the channel decoder is a highly nonlinear, on-off device, which only works if its input has a quality

exceeding a certain threshold, and this is not completely captured by the MSE. After such threshold is reached, a further improvement in the decoder input quality (as may be obtained by passing from $\theta = 10^{-6}$ to $\theta = 10^{-7}$) does not improve the BER anymore.

In Table I, we include the average number of receiver iterations, the average total number of steepest-descent steps and the SNR required for a BER of 10^{-4} in the case of other system setups, where there is either non-perfect CSI or a significant amount of fading (in all the cases, $\theta = 10^{-6}$). We have included for comparison the figures for the $K_{Rice} = 100$ dB case with $\theta = 10^{-6}$. As it can be expected, the SNR required grows as the detection or channel conditions get worse (i.e., lower E_C/E_s or lower K_{Rice}), reflecting what we can see in the previous figures. The number of receiver iterations lies always between 4 and 5, reflecting the fact that the genie-aided decoding stopping criterion is triggered at a similar point for a given BER, regardless of other conditions. In the case of the average total number of steepest-descent steps, we have another picture. For the channel with Rician fading and perfect CSI (cases (f) through (i)), we have a slight increase in the number of steps, as the process evolves towards the pure Rayleigh case. The small oscillation for $K_{Rice} = -10$ dB (with respect to the previous and subsequent K_{Rice} values) could be due to a statistical artifact related to the specific simulation.

If we focus on the non-fading non-perfect CSI setup results (cases (b) to (e)), we see that the trend is descending with lower values of E_C/E_s . This means that the number of steps required at a given BER decreases as the CSI estimation gets worse. The reason for this probably stands in the different behavior of the objective function (13) with lower E_C/E_s at the corresponding SNR. A higher amount of channel estimation noise is likely to smooth $h^{(l)}(\Phi)$, by filling the canyons and flattening the hills, thus yielding a faster convergence of the steepest-descent algorithm.

	(a)	(b)	(c)	(d)	(e)	(f)	(g)	(h)	(i)
E_s/N_0 dB	9.18	10.55	12.47	15.67	20.01	9.44	10.44	11.81	12.26
Av. RX iterations	4.65	5.09	4.62	4.12	4.40	4.46	4.93	4.72	4.95
Av. total no. SD steps	629.84	643.25	522.76	383.39	32.15	618.43	674.89	666.30	698.56

TABLE I

REQUIRED E_s/N_0 , AVERAGE NUMBER OF RECEIVER ITERATIONS AND AVERAGE TOTAL NUMBER OF STEEPEST-DESCENT STEPS AT AROUND 10^{-4} BER FOR THE CASES DEPICTED IN FIGS. 8 AND 9. CASE (a): PERFECT CSI AND $K_{Rice} = 100$ dB. CASES (b) – (e): NON FADING AND $\frac{E_C}{E_s} = 20, 15, 10$ AND 5 dB, RESPECTIVELY. CASES (f) – (i): PERFECT CSI AND $K_{Rice} = 10, 0, -10, -100$ dB, RESPECTIVELY.

D. Algorithm complexity and latency

The iterative receiver described in this paper has its core in the steepest-descent algorithm, used to solve the optimization problem in (11), in order to perform the phase estimation. In the previous subsection, we

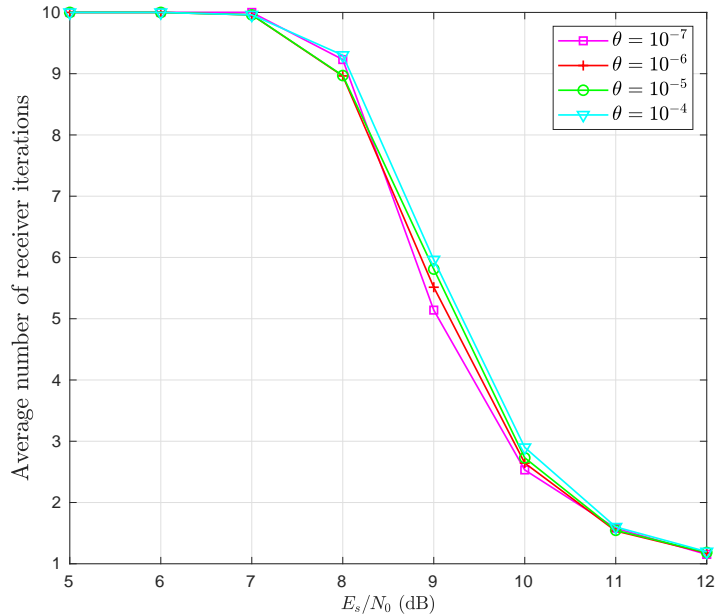


Fig. 10. Average number of receiver iterations for several cases with different thresholds θ for the steepest-descent gradient algorithm.

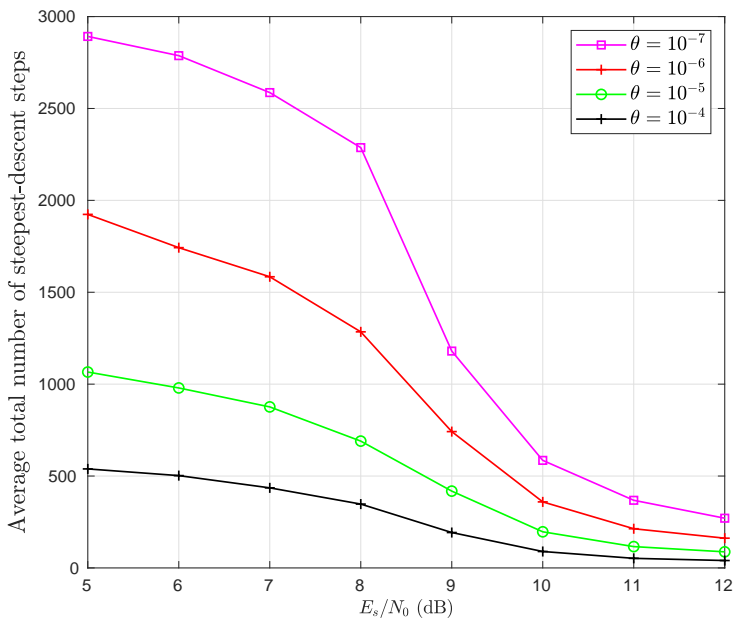


Fig. 11. Average total number of steepest-descent gradient steps required as a function of threshold θ for the same cases considered in Fig. 10.

have shown the average number of steepest-descent steps needed to trigger a convergence condition, as a function of threshold θ , in various settings. In each step, for every time n , (15) must be computed for each phase-noise atomic process at the transmitter, (16) for each process at the receiver. The additional computation related to phase-noise a-priori distribution (see (18)) is neglectable. Thus, we can make an estimate of the overall amount of computation needed as $O(N_r N_t (O_r + O_t) L \bar{I}_{SD})$, where \bar{I}_{SD} is the

average *total* number of steepest-descent steps in all receiver iterations. This detector complexity must be added to that of the other receiver blocks, especially of the channel decoder, which is typically the most complex block in the receiver. While this computational burden is not irrelevant, it has to be reminded that it is performed at the BS, where the hardware is usually powerful enough to bear it.

The proposed receiver requires a certain number of iterations, thus it may seem to pose some challenges regarding latency. However, considering Figure 10, we notice that it boils down to a noniterative receiver for a large enough SNR⁴. Therefore, our proposal could be conceived as a tool to reduce the operative SNR, with respect to a noniterative receiver, at the price of some latency increase. In addition, if we suppose that users have different channel SNRs, we can imagine that those of them with a larger SNR would be decoded faster than the others, thus configuring a dynamical trade-off between channel quality and experienced latency.

VI. CONCLUSIONS

In this article we have reviewed an EM-based algorithm for PN estimation and correction designed for a MIMO setup, and we have expanded its possibilities to cover massive MIMO cases with a generalized distribution of antennas and oscillators. We have also considered Rician block fading and the possibility to have imperfect CSI at the receiver side. As a result, we have proposed a generalized PN estimation algorithm able to compensate for each atomic PN process stemming from each oscillator (both at the transmitter and at the receiver side). We have also characterized the BCRB for this setup, so as to be able to compare performances in terms of the MSE attained.

The core of the algorithm comprises iterative reception, demodulation and decoding, as well as a steepest-descent gradient optimization stage with dynamic adaptation of the step and a stopping criterion based on a threshold. The iterative receiver itself implements a stopping rule based on the performance of the channel decoder. We have simulated a massive MIMO system with different channel conditions and different setup parameters. The MSE results have shown that the algorithm can approach the BCRB for low values of the steepest-descent gradient threshold, but with little or no gain in BER below a given value. The MSE and BER results obtained for the imperfect CSI case show how the CSI mismatch can degrade the performance significantly, and stresses the fact that a sufficiently good channel estimation is

⁴While we have used a genie-aided stopping rule to stop receiver iterations, a real stopping rule for channel decoders, e.g., LDPC decoders, performs in a similar way, just requiring a few more iterations on the average.

essential in massive MIMO frameworks. The presence of Rician block fading has also shown to hinder the performance, but with far less impact than in the case of imperfect CSI.

On the other hand, we have evaluated the number of receiver iterations and steepest-descent gradient algorithm steps required for given channel situations and specific configuration parameters. We have shown that it is possible to establish interesting trade-offs among MSE, BER and number of iterations/steps. In fact, by limiting the number of steepest-descent gradient algorithm steps with an appropriate choice of the threshold, it is still possible to attain the best BER performance despite slight degradations in MSE. All this shows that the proposed receiver can be proficient in counteracting the effects of PN in massive MIMO systems, with an affordable computational burden and a trade-off between latency and received SNR. Future work will be focused in expanding the study of the properties of the system, for example, providing insights on how different alternatives for the massive MIMO demodulator and the channel code may impact the PN estimation and compensation process.

REFERENCES

- [1] T. L. Marzetta, "Noncooperative Cellular Wireless with Unlimited Numbers of Base Station Antennas," *IEEE Trans. Wireless Commun.*, vol. 9, pp. 3590–3600, Nov. 2010.
- [2] T. K. Y. Lo, "Maximum ratio transmission," *IEEE Trans. on Commun.*, vol. 47, pp. 1458–1461, Oct. 1999.
- [3] E. Björnson, J. Hoydis, M. Kountouris and M. Debbah, "Massive MIMO Systems With Non-Ideal Hardware: Energy Efficiency, Estimation, and Capacity Limits," *IEEE Trans. Inf. Theory*, vol. 60, no. 11, pp. 7112–7139, Nov. 2014
- [4] A. Tarable, G. Montorsi, S. Benedetto and S. Chinnici, "An EM-based phase-noise estimator for MIMO systems," in *Proc. of the IEEE Int. Conf. on Commun. (ICC)*, 2013, pp. 3215–3219.
- [5] R. Krishnan, M. R. Khanzadi, N. Krishnan, A. Graell i Amat, T. Eriksson, N. Mazzali and G. Colavolpe, "On the Impact of Oscillator Phase Noise on the Uplink Performance in a Massive MIMO-OFDM System," *available at* <https://arxiv.org/abs/1405.0669>, 2014.
- [6] A. Pitarokoilis, E. Björnson and E. G. Larsson, "Performance of the Massive MIMO Uplink With OFDM and Phase Noise," *IEEE Commun. Lett.*, vol. 20, pp. 1595–1598, Aug. 2016.
- [7] A. Puglielli, G. LaCaille, A. M. Niknejad, G. Wright, B. Nikolić and E. Alon, "Phase noise scaling and tracking in OFDM multi-user beamforming arrays," 2016 *IEEE Intern. Conf. on Commun. (ICC)*, pp. 1–6, 2016.
- [8] R. Corvaja and A. G. Armada, "Phase Noise Degradation in Massive MIMO Downlink With Zero-Forcing and Maximum Ratio Transmission Precoding," *IEEE Trans. Veh. Technol.*, vol. 65, pp. 8052–8059, Oct. 2016.
- [9] X. Cheng, K. Xu and S. Li, "Compensation of Phase Noise in Uplink Massive MIMO OFDM Systems," *IEEE Trans. Wireless Commun.*, vol. 18, no. 3, pp. 1764–1778, Mar. 2019.
- [10] A. Pitarokoilis, S. K. Mohammed and E. G. Larsson, "Uplink Performance of Time-Reversal MRC in Massive MIMO Systems Subject to Phase Noise," *IEEE Trans. Wireless Commun.*, vol. 14, pp. 711–723, Feb. 2015.
- [11] R. Krishnan et al., "Linear Massive MIMO Precoders in the Presence of Phase Noise – A Large-Scale Analysis," *IEEE Trans. Veh. Technol.*, vol. 65, pp. 3057–3071, May 2016.

- [12] Y. -F. Wang and J. -H. Lee, "A ZF-Based Precoding Scheme With Phase Noise Suppression for Massive MIMO Downlink Systems," *IEEE Trans. Veh. Technol.*, vol. 67, no. 2, pp. 1158-1173, Feb. 2018.
- [13] X. Yang, S. Jin and C. -K. Wen, "Symbol Detection of Phase Noise-Impaired Massive MIMO Using Approximate Bayesian Inference," *IEEE Signal Process. Lett.*, vol. 26, no. 4, pp. 607-611, April 2019.
- [14] M. E. Rasekh, M. Abdelghany, U. Madhow and M. Rodwell, "Phase Noise in Modular Millimeter Wave Massive MIMO," *IEEE Trans. Wireless Commun.*, vol. 20, pp. 6522-6535, Oct. 2021.
- [15] R. Corvaja and A. G. Armada, "Analysis of SVD-Based Hybrid Schemes for Massive MIMO With Phase Noise and Imperfect Channel Estimation," *IEEE Trans. Veh. Technol.*, vol. 69, no. 7, pp. 7325-7338, July 2020.
- [16] B. Chatelier and M. Crussière, "On the Impact of Phase Noise on Beamforming Performance for mmWave Massive MIMO Systems," in *Proceedings of the IEEE Wireless Commun. and Networking Conf. (WCNC)*, 2022, pp. 1563-1568.
- [17] Y. Fang, L. Qiu, X. Liang and C. Ren, "Cell-Free Massive MIMO Systems With Oscillator Phase Noise: Performance Analysis and Power Control," *IEEE Trans. Veh. Technol.*, vol. 70, no. 10, pp. 10048-10064, Oct. 2021.
- [18] S. -N. Jin, D. -W. Yue and H. H. Nguyen, "Spectral Efficiency of a Frequency-Selective Cell-Free Massive MIMO System With Phase Noise," *IEEE Wireless Commun. Lett.*, vol. 10, no. 3, pp. 483-487, March 2021.
- [19] R. Zhang, B. Shim and H. Zhao, "Downlink Compressive Channel Estimation With Phase Noise in Massive MIMO Systems," *IEEE Trans. Commun.*, vol. 68, no. 9, pp. 5534-5548, Sept. 2020.
- [20] P. Zhang, J. Liu, Y. Shen and X. Jiang, "Exploiting Channel Gain and Phase Noise for PHY-Layer Authentication in Massive MIMO Systems," *IEEE Trans. Inf. Forensics Security*, vol. 16, pp. 4265-4279, 2021.
- [21] X. Zheng, A. Liu and V. Lau, "Joint Channel and Location Estimation of Massive MIMO System With Phase Noise," *IEEE Trans. Signal Process.*, vol. 68, pp. 2598-2612, 2020.
- [22] A. Tarable and F. J. Escribano, "Information aging in massive MIMO systems affected by phase noise," in *Proc. of the XXXIVth Gen. Assembly and Scientific Symp. of the Int. Union of Radio Science (URSI GASS)*, 2021, pp. 1-4.
- [23] J. Dauwels, S. Korl, and H.-A. Loeliger, "Expectation maximization for phase estimation," in *Proc. of the 8th Int. Symp. on Commun. Th. and Appl.*, 2005.
- [24] L. Armijo, "Minimization of functions having Lipschitz continuous first partial derivatives," *Pacific J. Math.*, vol. 16, no.1, pp 1-3, Jan. 1966.
- [25] J. Barzilai and J. M. Borwein, "Two-Point Step Size Gradient Methods," *IMA Journal of Numerical Analysis*, vol. 8, no. 1, pp. 141-148, Jan. 1988.
- [26] A. A. Nasir, H. Mehrpouyan, R. Schober and Yingbo Hua, "Phase noise in MIMO systems: Bayesian Cramer-Rao bounds and soft-input estimation," *IEEE Trans. on Sig. Proc.*, vol. 61, no. 10, pp. 2675-2692, May 2013.
- [27] A. Tarable, C. Camarda and G. Montorsi, "Cramer-Rao bounds for MIMO LOS systems affected by distributed Wiener phase noise in the large-blocklength regime," in *Proc. of the 6th Int. Symp. on Commun., Control and Signal Proc. (ISCCSP)*, 2014, pp. 97-100.
- [28] 3GPP TS 38.212. "NR; Multiplexing and channel coding." 3rd Generation Partnership Project; Technical Specification Group Radio Access Network.